

Investigation of Friction and Wear Properties of Duplex-Annealed Ti-6Al-2Sn-4Zr-2Mo Against Hardened AISI E52100 at Linear Reciprocating Motion

Sebastian Heilig¹ · Maziar Ramezani²  · Thomas Neitzert² · Mathias Liewald¹

Received: 16 October 2017 / Accepted: 18 December 2017 / Published online: 8 January 2018
© The Indian Institute of Metals - IIM 2018

Abstract Near- α titanium alloys possess enhanced properties such as high specific strength, low density, corrosion resistance and an excellent creep behaviour at high operating temperatures which makes them suitable for a wide range of aerospace application areas. However, titanium and its alloys are known for their poor tribological properties which limit their applicability to structural materials. Due to increasing demands on efficiency and environmental restrictions, the application of Ti-6Al-2Sn-4Zr-2Mo as bearing material should also be considered. Experiments were performed on a linear reciprocating tribometer for a constant sliding distance of 300 m, a fixed stroke of 10 mm, at normal loads between 5 and 20 N varying the frequency between 2 and 4 Hz. For the lubrication tests a biodegradable hydraulic oil based on synthetic esters was applied between the two solid bodies. Mechanical properties of the tribotechnical system were determined by tensile tests, hardness and roughness tests as well as microstructural observations. Under dry condition, the Coefficient of Friction (CoF) decreases with increasing load and increasing frequency, whereas the wear volume increases with increasing load and decreasing frequency. Generally, the CoF significantly decreases by applying a lubricant and tends to increase with increasing load and increasing frequency whereas the wear volume increases at higher loads and frequencies. The protective effect of the lubricant against wear is absent. Either the wear volume

shows the same values or possesses higher values compared to dry condition. The occurring wear mechanism was determined using a scanning electron microscope to observe the wear track and conduct an elemental analysis using energy-dispersive X-ray spectroscopy.

Keywords Linear reciprocating tribometer · Ti-6Al-2Sn-4Zr-2Mo · Tribology · Wear

1 Introduction

Ti-6Al-2Sn-4Zr-2Mo (Ti-6-2-4-2) is a near- α high-strength titanium alloy developed for elevated temperature applications at which the most common $\alpha + \beta$ titanium alloy Ti-6Al-4V (Ti-6-4) deteriorates due to its poor creep and oxidation resistance [1–4]. The major application field of Ti-6-2-4-2 can be found in aircraft constructions. Gas turbine engine components like discs, impellers, compressor blades, high performance automobile valves, cam and followers and pistons, and sheet metal components like afterburner cans and hot airframes are also made out of Ti-6-2-4-2 [5, 6]. The replacement of former aerospace materials like higher strength steels, aluminium and nickel-based superalloys with titanium alloys have achieved great advantages e.g. weight reduction, higher strength and furthermore improves resistance to creep, oxidation and corrosion [3, 5]. Concerning the mechanical properties, Ti-6-2-4-2 shows an outstanding combination due to its high strength to weight ratio, low density, exceptional corrosion and creep resistance and furthermore high temperature stability for long term applications up to 565 °C [1, 3, 5, 7, 8].

The mechanical properties depend mainly on the microstructure, the chemical composition and the

✉ Maziar Ramezani
maziar.ramezani@aut.ac.nz

¹ Institute for Metal Forming Technology, University of Stuttgart, 70174 Stuttgart, Germany

² Department of Mechanical Engineering, Auckland University of Technology, Auckland 1010, New Zealand

thermomechanical treatment during processing [3, 6]. The alloying elements can be divided into two stabilizer types. Ti-6-2-4-2 contains 6% Aluminium as a potent α -stabilizer which raises the beta transus temperature, whereas 2% Molybdenum as a β -stabilizer makes the β -phase appear at lower temperatures. The α -phase has a hexagonal closed packed structure (hcp) which is characterised by lower density, higher strength and lower ductility compared to the body centred cubic (bcc) β -phase [1, 3, 4]. Tin has a neutral effect on the β -transus temperature and promotes the formation of precipitates which act as a barrier for dislocation glide and climb [2]. In some cases, silicon is added to improve the creep resistance. It precipitates as silicide along the grain boundaries of the $\alpha - \beta$ interface and hinders dislocating motion at higher temperatures up to 520 °C [1, 2]. The high temperature resistance is achieved by the formation of a thermally stable oxide film decreasing the oxygen diffusion rate. Furthermore, the TiO₂ layer supplies corrosion resistance so that painting gets unnecessary except in galvanic corrosion cases [3].

Fine, equiaxed microstructures with lower grain sizes increase the strength and ductility, retard crack nucleation and support superplastic behaviour, while coarse and lamellar microstructures are more resistant to creep and fatigue crack growth [3, 8, 9]. Concerning friction and wear, only few papers about Ti-6-2-4-2 are available, whereas the tribology of the most commonly used alloy Ti-6-4 has been studied extensively. Zhong et al. [10] investigated the wear behaviour of Ti-6-4 in vacuum condition and Wang et al. [11] did an experimental investigation using a pin-on-disc tribometer with temperatures up to 600 °C. Mao et al. [12] concluded, that the wear resistance at 400–500 °C is improved due to the appearance of hard oxides, which play a protective role. Regarding the near- α alloy Ti-6-2-4-2, the research has been focused mainly on the oxidation behaviour and the formation of the α -case layer. Investigations on temperature effects, oxidation kinetics, diffusion rates have been made [2, 13, 14]. Additionally, the stress corrosion cracking behaviour and the use of Ti-6-2-4-2 in hot sheet metal forming has been investigated [8]. The solid film lubrication by an h-BN coating applied by polymer derived ceramic for higher temperature tribology has been studied by Yuan et al. [15]. Qu et al. [16] conducted friction and wear tests with Ti-6-2-4-2 discs against a 440C stainless steel ball at ambient temperature. He concluded, that wear as well as the coefficient of friction decrease with increasing sliding speed. High sliding speed causes higher surface temperatures and reduces shear strength though.

Despite these published papers, a systematic approach towards the influence of key process parameters, e.g. normal load, sliding speed and surface contact conditions on

tribological performance of Ti-6-2-4-2 alloy is still missing which is the main reason for the current research. An investigation of wear mechanism of this material is another motivation of this research that has been done by microscopic studies. The results can be useful for designing Ti-6-2-4-2 alloy for applications with sliding contacts.

2 Materials and Experimental Procedure

The Titanium alloy was received as hot rolled duplex-annealed sheet with a thickness of 1.6 mm. The bearing ball material was AISI E52100 steel, hardened to 58HRC with a diameter of 10 mm. The chemical compositions of the mating materials are summarized in Table 1.

The friction and wear tests were conducted on a Ducom TR-282 Linear Reciprocating Tribometer (LRT). The experimental procedure was based on ASTM International standard test method for linearly reciprocating ball-on-flat sliding wear [17]. The stroke length was kept constant at 10 mm while the frequency was varied between 2 and 4 Hz under different applied loads between 5 and 20 N. All tests were performed until a sliding distance of 300 m was reached. In case of lubricated tests, a synthetic ester hydraulic oil was applied between the two mating surfaces. It is worth pointing out that most applications of Ti-6-2-4-2 are for dry contact conditions; however some applications such as high performance piston valves and pistons work under lubricated contact conditions. Because of this, the tests were conducted both dry and lubricated contact conditions.

To achieve higher reproducibility, each test was iterated three times. The titanium sheets were cut with Electrical Discharge Machining (EDM) into quarters (39.8 × 39.8 mm). Due to surface scratches and printings on the received sheet, a surface finish was necessary for similar and reproducible surface conditions. The quarters were grinded with a wet SiC 1000 grid paper and the average roughness was measured using a Taylor Hobson Form Talysurf 50 profilometer. The output parameters of the reciprocating tests were frictional force and Coefficient of Friction (CoF). The wear volume was calculated over the mass loss and density. The density of Ti-6-2-4-2 is 4.45 g/cm³ [4] and the density of AISI E52100 is 7.81 g/cm³ [18].

$$\Delta V = \Delta m / \rho \quad (1)$$

The mass loss was determined by weighing the samples before and after the tests. To gain more accurate result, the samples were cleaned before weighing. Cleansing by an 80% ethanol was used for the removal of debris or contamination of the surface finish or the wear process. In the following, the samples were weighted by a Mettler

Table 1 Chemical composition of the materials [4, 18]

| | Composition (wt%) | | | | | | | | | | | | | |
|-------------|-------------------|------|----|----|----|----|------|------|----------|---------|-------|----------|---------|-----------|
| | Ti | Fe | Al | Sn | Zr | Mo | N | O | C | P | S | Si | Cr | Mn |
| Ti-6-2-4-2 | 86 | 0.25 | 6 | 2 | 4 | 2 | 0.04 | 0.15 | – | – | – | 0.08 | – | – |
| AISI E52100 | – | 97 | – | – | – | – | – | – | 0.95–1.1 | 0–0.025 | 0.025 | 0.2–0.35 | 1.3–1.6 | 0.25–0.45 |

Toledo analytical balance with an accuracy of 0.1 mg. The specific wear rate k , which describes the sliding wear was calculated using the simplified Archard equation in dependency of the wear volume ΔV , the normal load F_n and the sliding distance L [19]:

$$k = \Delta V / F_n L \quad (2)$$

The wear mechanisms were determined by observations of the surface topography and an elemental analysis using a Hitachi SU-70 scanning electron microscope (SEM) combined with energy dispersive spectrometry (EDS). For the metallographic preparation, small quarters (10 × 10 mm) of the wear track were separated by a Struers 40A25 water cooled cut off wheel. Thereafter, either the cross sections or the surface track sections were mounted with a Struers PolyFast hot mounting resin at 180 °C for a duration of 2 min. The grinding was conducted on a rotary grinder with SiC grinding papers in the sequence of P180, P500, P1200 and P2400 grid. Afterwards, the samples were polished on a Struers synthetic MD-Nap cloth with firstly 6 μm and secondly 1 μm diamond paste including the application of a 3% H₂O₂ solution. The etching was performed by submerging the samples in Kroll's reagent which contained 2% HF, 6% HNO₃ and 92% distilled H₂O for a duration of about 10 min. Mechanical properties of the received Ti-6-2-4-2 material were also determined using tensile tests. Tensile tests were based on the ASM International standards using pin gripped dog bones with a gage length of 10 mm and a constant strain rate of 0.03/s [20]. The indentation hardness was measured using a Rockwell Hardness tester. Furthermore, the contact pressure in dependency of the applied normal load was calculated by the Hertzian pressure equation for a ball-on-flat case [21].

3 Results and Discussion

This chapter is divided into three subsections. Firstly, the properties of the TTS which influence the output variables as well as the loss variables are illustrated. Secondly, the behaviour of the CoF will be discussed for both dry and lubricated contact condition. The last section is about wear.

Occurring wear volumes and wear scars are discussed and the wear mechanisms are determined using SEM and EDS.

3.1 Tribotechnical System (TTS) Properties

The microstructure of the as-received Ti-6-2-4-2 is shown in Fig. 1. A fine microstructure with grain sizes in the range of 20 μm can be observed. The α – β phase is dominated by the harder α -grains due to the content of 6% Aluminium as an α -stabilizer. The content of 2% Molybdenum as a β -stabilizer makes transformed β -grains appear at lower temperatures. Additionally, precipitation can be observed on the α – β phase.

The indentation hardness for both materials is measured by a Rockwell test under the respective Rockwell scale HRC with an applied major load of 150 kgf. The surface roughness is represented by the arithmetic average of the absolute values, R_a , after the surface finish. The results are given in Table 2.

The Ti-6-2-4-2 sheets possess distinctly lower hardness values and higher roughness values compared to the bearing balls out of AISI E52100. To gain the material properties e.g. Yield Strength (YS) and Ultimate Tensile Strength (UTS), tensile tests have been performed at ambient temperature with a strain rate of 0.03/s with three iterations. The tensile test specimen dimensions, which are

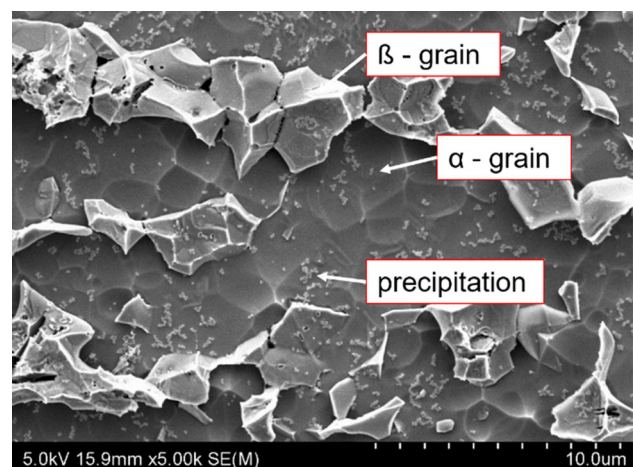


Fig. 1 SEM picture of the microstructure of duplex-annealed Ti-6-2-4-2 at a magnification of 5000

Table 2 Average Rockwell hardness (HRC) and roughness R_a of the mating materials

| Material | Hardness (HRC) | Roughness R_a (μm) |
|-------------|----------------|-----------------------------------|
| Ti-6-2-4-2 | 35.1 ± 1.2 | 0.4 ± 0.12 |
| AISI E52100 | 58.0 ± 1.5 | ($\ll 0.4$) |

illustrated in Table 3, comply with the ASTM E8 standard [20].

The engineering stress strain diagram is illustrated in Fig. 2.

The average tensile test results are summarized in Table 4 in comparison to properties of AISI E52100. Concerning the fracture surface, Ti-6-2-4-2 shows a quite ductile fracture mode containing dimples with a diameter of 20–30 μm and microvoids with a width of 5–10 μm .

The contact stress S_c within the mating solids is calculated by the elastic Hertzian contact stress theory for a sphere-on-flat case with the composite modulus E^* , the

Poisson's ratio of each body $\nu_{1/2}$, the normal force F_n and the diameter of the ball D [21].

$$S_c = 0.918(F_n/DE^*)^{1/3} \quad (3)$$

$$E^* = (1 - \nu_1)/E_1 + (1 - \nu_2)/E_2 \quad (4)$$

The resulting contact stresses for each applied normal load are summarized in Table 5. It is worth mentioning that the Hertzian contact pressure is not proportional to the applied load and is only valid for the beginning of the test before any wear taking place (for elastic deformation case). It should also be noted that the applied load of 20 N results in a contact stress of 995.52 MPa which is above the ultimate tensile strength of Ti-6-2-4-2 alloy. However, the calculated Hertzian contact pressure is just an indication of real contact stress and only valid for elastic deformation. No permanent deformation is observed on the surface of the test pieces after applying the 20 N loads and before running the sliding wear tests. 20 N loading

Table 3 Dimensions of a tensile flat test specimen in mm

| Gauge length | Width | Thickness | Fillet radius | Overall length | Length of reduced section | Length of grip section |
|--------------|-------|-----------|---------------|----------------|---------------------------|------------------------|
| 8 ± 0.01 | 1.5 | 1.6 | 1 | 75 | 13 | 30 |

Table 4 Average tensile properties with their standard deviations

| | Yield strength (MPa) | Ultimate tensile strength (MPa) | Youngs modulus (GPa) | Total strain (%) | Poisson's ratio |
|-------------|----------------------|---------------------------------|----------------------|------------------|-----------------|
| Ti-6-2-4-2 | 933.3 ± 7.4 | 966 ± 7.1 | 112.8 ± 1.2 | 29.4 ± 0.01 | 0.32 |
| AISI E52100 | – | – | 200 | – | 0.3 |

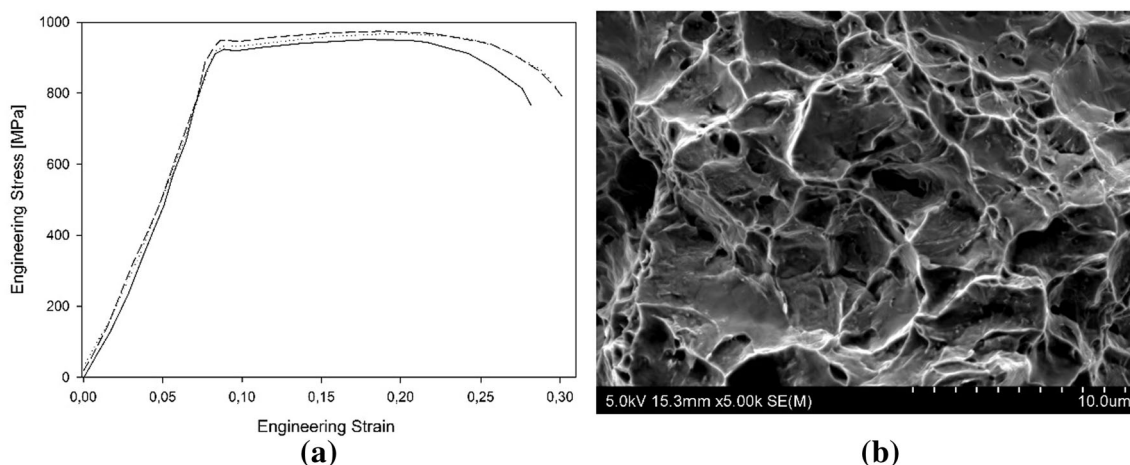


Fig. 2 Engineering Stress–Strain diagram for duplex-annealed Ti-6-2-4-2 at a strain rate of 0.03/s and a typical SEM image of the dog bone fracture surface with a magnification of 5000. **a** Stress–Strain diagram and **b** dog bone fracture surface

Table 5 Hertzian contact stress between an AISI E5200 sphere on a Ti–6–2–4–2 flat

| Applied load F_n (N) | 5 | 10 | 15 | 20 |
|----------------------------|--------|--------|-------|--------|
| Contact stress S_c (MPa) | 627.14 | 790.15 | 904.5 | 995.52 |

condition can actually be considered as near the onset of yield for this material and for this specific test set-up.

3.2 Friction

The mean CoF values for different loads and frequencies under dry and lubricated sliding conditions are illustrated in Fig. 3. Under dry contact condition, the CoF generally reaches higher values compared to lubricated condition. The application of a lubricant results in a decreasing resistance against movement. The CoF slightly increases with increasing load and tends to be higher at higher frequencies. As can be seen in Fig. 3, three normal loads of 10, 15 and 20 N have been selected for comparison between dry and lubricated contact conditions. A normal load of 5 N has also been tried for lubricated condition, but the sensor is unable to indicate a friction force due an occurring hydrodynamic lift force at this loading case for frequencies of 2 and 4 Hz, corresponding to the sliding speeds of 40 and 80 mm/s respectively. This speed range is comparable to practical applications such as cam follower system, or a deep drawing process. These two frequencies have been selected based on the range of real applications of this alloy as well as limitations of the tribometer.

The application of a biodegradable synthetic ester lubricant effects lower sliding resistance. Related to dry sliding, the effects of the varied input parameters like load and frequency on the CoF are different. Concerning dry sliding, the CoF tends to be higher at lower frequency,

whereas lower frequencies under lubricated condition cause minor resistance to movement. Furthermore, the CoF decreases with increasing load under dry sliding, whereas it remains constant or slightly increases under lubricated conditions. Figure 4 illustrates the course of the CoF over the sliding distance under dry and lubricated condition.

The curve of the CoF under dry condition is characterized by a short break-in with the lowest CoF followed by a transition process with increasing CoF values. The steady state sets in after 80 m sliding distance, categorized with the highest CoF values and massive fluctuations. Under lubricated contact condition, lower CoF values and little fluctuations as well as a different curve shape compared to dry conditions can be recognized. The run-in process is characterized by decreasing CoF values to about 200 m. Whereas in dry condition, the CoF increases towards the steady state reaching its maximum values, the CoF under lubricated condition achieves its lowest values with lower fluctuations. The initial surface roughness is worn off, leaving smoother surfaces and results in a reduction of friction.

3.3 Wear

The wear volumes as well as the wear rates under dry and lubricated sliding conditions are illustrated in Fig. 5. In general, the wear volume tends to increase with higher load, whereas the effect of lubrication and frequency is different. Regarding dry sliding, a low frequency (2 Hz)

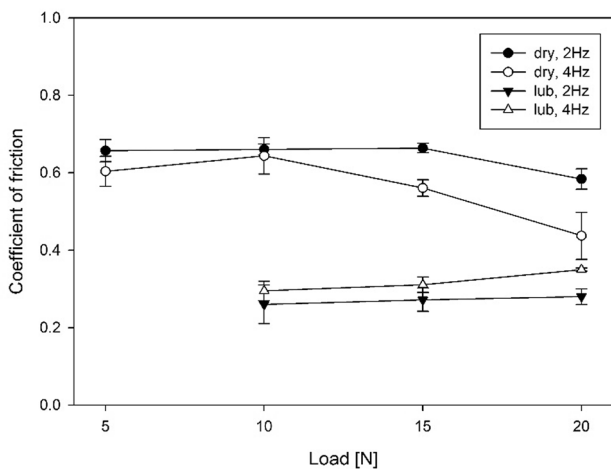


Fig. 3 Mean values of CoF over the applied load under dry and lubricated contact condition with frequencies of 2 and 4 Hz

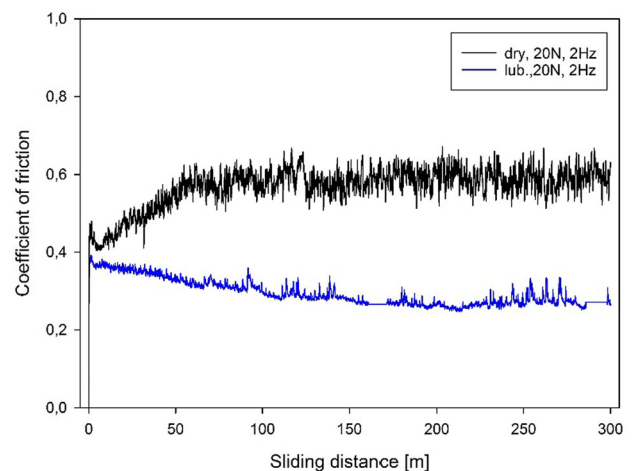


Fig. 4 Coefficient of friction over sliding distance under dry and lubricated contact condition under 20 N load and 2 Hz frequency

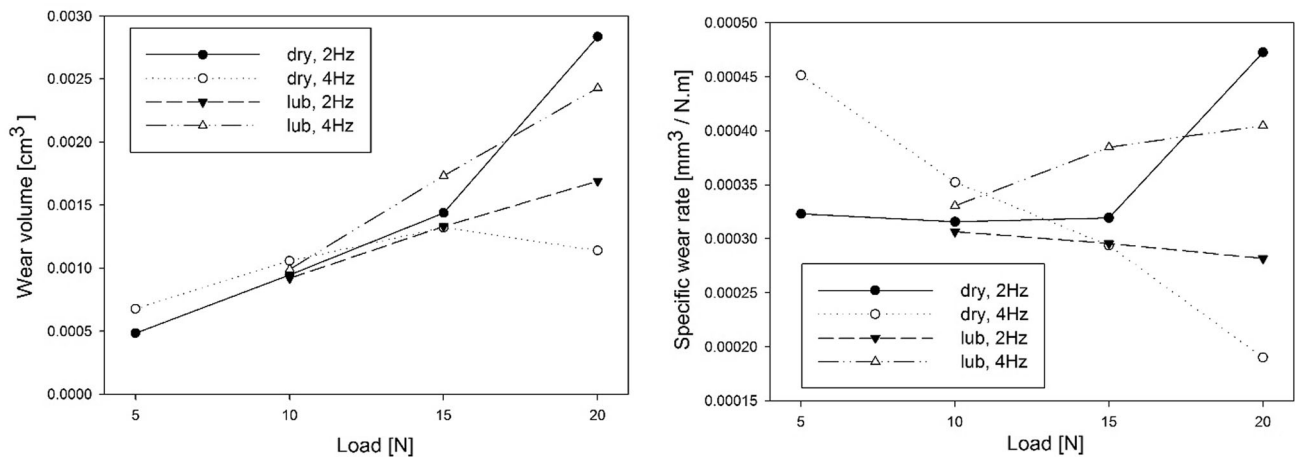


Fig. 5 Wear volumes and specific wear rate in dependency of the applied normal load and frequency under dry and lubricated contact conditions

results in less wear in case of lower loads and outcomes with high wear volumes for higher loads. This is also supported by the specific wear rate. The curve of 2 Hz under dry sliding rises with increasing load above 15 N. The wear rate at 4 Hz under dry sliding decreases with increasing load and results in the minimum wear volume of all tests under the maximum applied load of 20 N. In case of lubricated tests, the protective function of the lubricant against occurring wear is absent. The occurring wear volume corresponds approximately to the resulting wear volumes at dry conditions. The wear volume increases with increasing load while higher frequencies lead to higher wear volumes. This can also be confirmed regarding the wear rate. With increasing load, a higher frequency (4 Hz) increases the wear rate whereas a lower frequency (2 Hz) shows a decreasing wear rate. Compared to dry sliding a reverse effect of the frequency with increasing load on the occurring wear can be determined. With increasing loads, the wear rate is more sensitive to the frequency. In case of dry sliding with 20 N load, the wear volume at 2 Hz is significantly higher compared to 4 Hz.

Figure 6 illustrates various cross sectional scans of the wear scar in dependency of lubrication and applied load. It can be stated, that the valley deepness increases with increasing load. Concerning 10 N load, the valley deepness after lubricated sliding is significantly higher compared to dry sliding, whereas the deepness of dry and lubricated sliding almost concurs at higher loads. Additionally, material attachments can be found at the edges of the cross sections under dry sliding. To determine the occurring wear mechanism, the wear track is observed using a SEM including EDS for elemental analysis. Pictures of the wear track topographies are displayed in Fig. 7 for different loads under dry and lubricated contact condition. Considering dry sliding, the wear track is dominated by abrasion grooves. The harder counter body made out of AISI

E52100 (58HRC) plunges into the softer sheet made out of Ti-6-2-4-2 (35 HRC). Additionally, delaminated platelets, adhesive material as well as oxidative areas can be detected on the surface. The occurrence of several mechanisms such as abrasion, adhesion, delamination and tribo-oxidation is designated as a Mechanically Mixed Layer (MML). The white spots in Fig. 7a, c are oxide layers created on the surface of the wear track, while the loose particles and the rough fractured areas show the presence of abrasion and adhesion mechanisms. For lubricated tests, the grooves and fractured areas in Fig. 7b, d are showing adhesion and delamination.

With increasing load, abrasion grooves grow in their width. The atomic percentage of oxygen increases, whereas the atomic percentage of the elements like iron and oxygen decreases. It can be inferred that with an increase in the applied load, oxidative and adhesive wear increases while the abrasion mechanism is still predominant. Regarding lubricated sliding motion, abrasion is the main wear mechanism. Very fine abrasion grooves with a typical width in the range of 10–20 μm can be detected at all loading conditions. With increasing normal load, the grooves appear more significant and furthermore very little areas with detached platelets occur on the wear track. The predominance of abrasion without oxidation and adhesion is supported by the elemental analysis of the EDS. Oxygen and iron couldn't be detected whereas nitrogen with an atomic percentage in the range between 5 and 7% has appeared. The atomic percentage of identified elements are summarized in Table 6.

4 Conclusions

1. Properties of the TTS like microstructure, deformation and fracture features, hardness, roughness and the

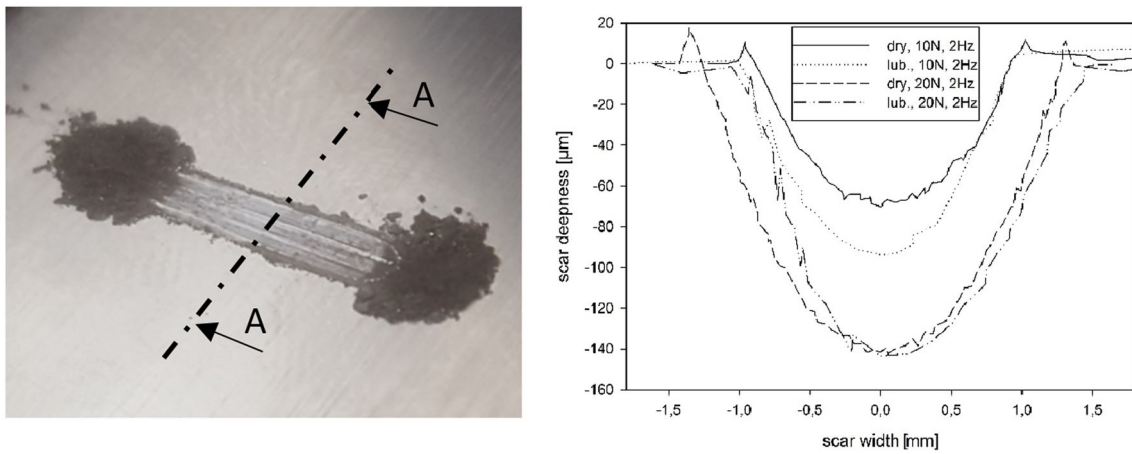


Fig. 6 Cross sectional scan of the wear scar for different loads under dry and lubricated contact conditions using a profilometer

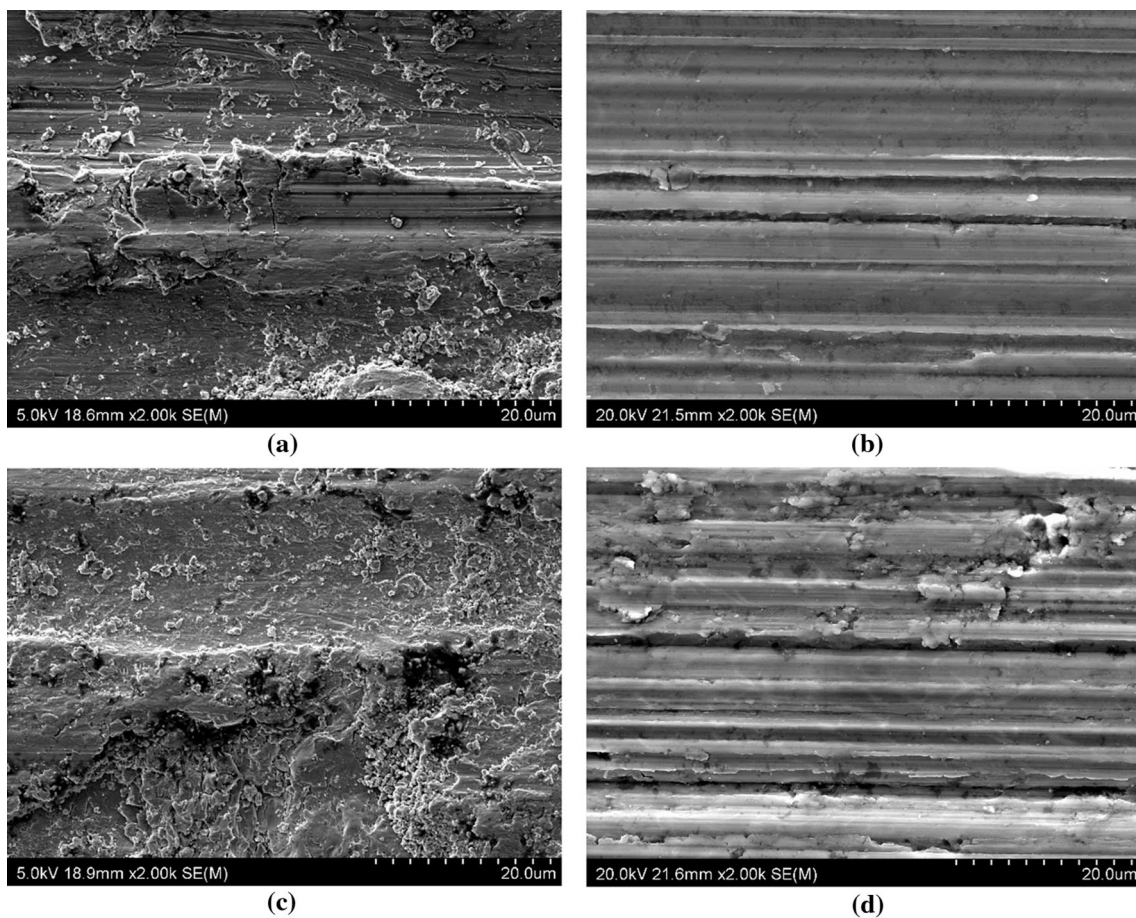


Fig. 7 SEM images of the wear track under linear reciprocating sliding with 2 Hz frequency under dry and lubricated contact conditions for 10 and 20 N applied load. **a** Dry condition, 10 N load, **b** lubricated condition, 10 N load, **c** dry condition, 20 N load and **d** lubricated condition, 20 N load

contact pressures have been investigated due to their significant influence on friction and wear.

2. Concerning the resistance against motion, dry contact conditions result generally in higher CoF values.

Table 6 Atomic percentage of detected elements on the wear surface in dependency of load and under dry and lubricated contact conditions using EDS allocated to the cases a–d of Fig. 7

| Load (N) | Lubrication | O | Al | P | S | Ti | Cr | Fe | Sn | Mo | N |
|----------|-------------|-------|------|------|------|-------|------|-------|------|------|------|
| 10 | Dry | 11.97 | 3.89 | 0.96 | 0.3 | 64.56 | 0.24 | 17.58 | 0.48 | 0.48 | 0.48 |
| 20 | Dry | 9.18 | 5.16 | – | 0.29 | 75.61 | 0.14 | 8.47 | 0.46 | 0.62 | – |
| 10 | Lubricated | – | 5.88 | 1.29 | – | 86.98 | – | – | 0.63 | – | 5.22 |
| 20 | Lubricated | – | 6.35 | 1.5 | – | 83.19 | – | – | 0.71 | 1.01 | 7.24 |

Additionally, the CoF decreases with increasing load and tends to be higher at lower frequencies. The CoF reaches its steady state after 100 m sliding distance towards maximum CoF values. Regarding the effectiveness of the applied lubricant in the form of a synthetic ester oil, the resistance to movement decreases. The CoF slightly increases with increasing load and tends to be higher at higher frequency. The CoF reaches its steady state after 200 m sliding distance resulting in the minimum CoF values.

- The wear volume of both dry and lubricated sliding condition increases with increasing load and are generally in the same range. This is also supported by cross sectional profilometer scans. Concerning dry condition, low frequencies result in less wear for lower loading forces, whereas high frequencies are more preventive for higher loads. In case of lubricated sliding, high frequencies generally result in higher wear, whereas lower frequencies result in a decreasing wear rate with increasing load. Concerning the wear volume, dry and lubricated sliding indicate approximately identical values. That means, that the protective effect of the lubricant against wear is absent.
- A Mechanically Mixed Layer (MML) consisting of abrasive grooves, adhesive regions and oxidized surfaces can be found under dry condition. With increasing load, the stake of adhesion and abrasion decreases while the abrasive grooves grow in their size. In case of lubrication, the predominant wear mechanism consists of abrasive grooving and ploughing where oxidation as well as adhesion is absent.

References

- Chamanfar A, Pasang T, Ventura A, and Misiolek W Z, *Mater Sci Eng A* **663** 213 (2016).
- Pustode M D, and Raja V S, *Metall Mater Trans A* **46** 6081 (2015).
- Veiga C, Davim J P, and Loureiro A J R, *Rev Adv Mater Sci* **32** 14 (2012).
- Boyer R, Welsch G, and Collings E W, *ASM Int Mater Inf Soc* ISBN: 978-0-87170-481-8 (1994).
- Prasad E, and Wanhill R J H, *Aerospace Materials and Material Technologies, Indian Institute of Metals Series*, Springer, Singapore ISBN 978-981-10-2134-3_5 (2017).
- Jia W, Zeng W, and Yu H, *Mater Des* **58** 108 (2014).
- Dupressoire C, Put A R-V, Emile P, Archambeau-Mirguet C, Peraldi R, and Monceau D, *Effect of Nitrogen on the Kinetics of Oxide Scale Growth and of Oxygen Dissolution in the Ti6242S Titanium-Based Alloy*, Springer, New York (2017).
- Odenberger E-L, Pederson R, and Oldenburg M, *Mat Sci Eng A* **489** 158 (2008).
- Tarin P, Rodriguez M C, Simon A G, Badia J M, and Antoranz J M, *Proc Inst Mech Eng* **220** 241 (2006).
- Zhong H, Dai L Y, Yue Y, Zhang B, Feng Z H, Zhang X Y, Ma M Z, Khosla T, Xiao J, and Liu R P, *Tribol Int* **109** 571 (2017).
- Wang L, Zhang Q Y, Li X X, Cui X H, Wang S Q, *Metall Mater Trans A* **45A** 2284 (2014).
- Mao Y S, Wang L, Chen K M, Wang S Q, and Chui X H, *Wear* **297** 1032 (2013).
- Gaddam R, Sefer B, Pederson R, and Antti M-L, *Mater Charact* **99** 166 (2015).
- McReynolds K S, and Tamirisakandala S, *Metall Mater Trans A* **42** 1732 (2011).
- Yuan S, Toury B, and Benayoun S, *Surf Coat Technol* **272** 366 (2015).
- Qu J, Blau P J, Watkins T R, Cavin O B, and Kulkarni N S, *Wear* **258** 1348 (2005).
- ASTM International G133-02, *Standard Test Method for Linearly Reciprocating Ball-on-Flat Sliding Wear*, West Conshocken (2002).
- Guo Y B, and Liu Y B, *J Manuf Sci Eng* **124** 1 (2002).
- ASM International Handbook 18, *Friction, Lubrication and Wear Technology*, ASM International Handbook 18 ISBN: 0-87170-380-7 (1992).
- Davis J R *Tensile Testing*, 2nd Edition, ASM International ISBN: 978-0-87170-806-9 (2004).
- Blau P J, *Friction Science and Technology*, Taylor & Francis Group, Boca Raton ISBN: 978-1-4200-5404-0 (2009).